Korean J. Chem. Eng., **31**(1), 29-36 (2014)
DOI: 10.1007/s11814-013-0185-6

pISSN: 0256-1115
eISSN: 1975-7220

Additive effect of Ce, Mo and K to nickel-cobalt aluminate supported solid oxide fuel cell for direct internal reforming of methane

Bu Ho Kwak*, Jungdeok Park*, Heechul Yoon*, Hyeon Hui Kim*, Lim Kim*, and Jong Shik Chung*,,†**

*Department of Chemical Engineering, POSTECH, Pohang 790-784, Korea
**School of Environmental Science and Engineering, POSTECH, Pohang 790-784, Korea
(*Received 6 November 2012 • accepted 26 September 2013*)

Abstract−Direct internal reforming of methane (steam/carbon=0.031, 850 °C) is tested using button cells of Ni-YSZ/YSZ/LSM in which the anode layer is supported either on Ni-YSZ or on Ni-$CoAl_2O_4$. The Ni-$CoAl_2O_4$ supported cell shows little degradation with operating time, as a result of higher resistance against carbon deposition, whereas the Ni-YSZ supported cell deactivates quickly and suffers fracture in 50 h. Upon incorporation of additives such as K, Ce, or Mo into the Ni-$CoAl_2O_4$ support, cells with 0.5 wt% CeO_2 exhibit the best stable performance as a result of reduced coke formation. Cells with 0.5 wt% Mo exhibit the lowest performance. Although no carbon deposit is detected in the cells with K_2CO_3 additives, their performance is worse than that in the CeO_2 case, and, in constant-current mode, there is a sudden voltage drop to zero after a certain period of time; this time becomes shorter with increasing K content. The injection of potassium into the anode side facilitates the generation of OH^- and CO_3^{2-} in the anode and promotes the diffusion of these ions to the cathode. Increased polarization resistance at the cathode and increased electrolyte resistance result in such a sudden failure.

Keywords: Solid-oxide Fuel Cell, Nickel-cobalt Aluminate Support, Direct Internal Reforming, Effect of Cerium, Molybdenum and Potassium

INTRODUCTION

Practical near-term applications of solid-oxide fuel cells (SOFCs) will need to use more easily available hydrocarbons such as methane (CH_4) directly because they are cheap and abundant, with the supply infrastructures already existing in many places. Direct internal reforming (DIR) of methane in the SOFC anode side has many attractive features: elimination of an external reformer, higher fuel-use efficiency, and, most of all, a good thermal balance between endothermic reforming and exothermic fuel cell reactions, which would be advantageous in making larger cells. Internal reforming of methane can take place easily in the anode side because of the high operating-temperatures of SOFCs, but practical applications are still a long way off because of severe coking problems encountered over Ni catalysts.

Steam reforming, one of the most common ways of using methane, can be expressed by Eq. (1):

$$CH_4+H_2O\leftrightarrow CO+3H_2 \quad (1)$$

The kinetics of steam reforming and the possibility of internal steam reforming on Ni-YSZ cermets with a high steam/carbon ratio (more than 2) have also been reported by many researchers [1,7]. For methane/steam reforming, Ni-alumina catalysts such as Ni-Al_2O_3, Ni-$NiAl_2O_4$, and Ni-$CoAl_2O_4$ are well known to be very active [8,9]. The Ni-$NiAl_2O_4$ and Ni-$CoAl_2O_4$ anode supports that exhibited good cell performance in hydrogen-fueled SOFCs [10] might therefore be good candidates for DIR operation. The carbon-deposition problems that inevitably occur over Ni can be suppressed to some degree by adding a small amount of an additive that is effective for carbon removal. For example, the incorporation of a small amount of gold or molybdenum into Ni-YSZ leads to a significant reduction in carbon deposition when operating at low steam/carbon ratios [2-6]. The addition of CeO_2 to the Ni-YSZ anode or Ni-Al_2O_3 support is also reported to provide high resistance against carbon deposition [7-9,11-13]. Potassium additives are well known to eliminate the formation of carbon in steam reforming [14-18]. However, there has been no investigation of the effects of these metal additives (K, Ce, and Mo) on Ni anodes in SOFC cells.

We investigated Ni-YSZ and Ni-$CoAl_2O_4$ as anode supports of Ni-YSZ for direct internal reforming at a low steam/methane ratio of 0.031. We also investigated the incorporation of a small amount of a coke-suppressing additive such as Ce, K, or Mo to the support to improve the performance and stability of the cell. Cell performance and stability can be correlated with the types and amounts of coke. Some interesting features induced when the support was impregnated with a potassium precursor were studied in more detail to reveal a sudden failure of the cell with an increase in the operating time.

EXPERIMENTAL

1. Sample Preparation and Characterization

The fabrication of Ni-YSZ- or Ni-$CoAl_2O_4$ supported cells has been described in detail in previous work [10]. NiO-YSZ and NiO-$CoAl_2O_4$ supports were prepared by mixing YSZ and $CoAl_2O_4$ powder with NiO powder (>99%, J.T. Baker), pressing the mixed powder into pellets of diameter 20 mm and pre-sintering at 1,100 °C for 2 h. To make a thin anode and electrolyte layer, NiO-YSZ (50 : 50 wt%)

†To whom correspondence should be addressed.
E-mail: jsc@postech.ac.kr

powder and YSZ powder were deposited one by one by a dip-coating technique and then co-sintered at 1,400 °C for 3 h. A mixture of LSM-YSZ and pure LSM ($(La_{0.8}Sr_{0.2})_{0.98}MnO_3$, NexTech Materials, Ltd.) powder was used as the cathode-side material. The cathode powder (90 wt%), polyvinyl butyral (5 wt%), and polyethylene glycol (5 wt%) were mixed together in isopropanol and ball-milled for 12 h to make a slurry. The slurries of LSM-YSZ and LSM were coated (0.7×0.7 cm^2) one by one onto the electrolyte film by stencil printing and fired at 1,200 °C for 3 h in air.

Metal-additive-injected cells were prepared using potassium carbonate (99.0% K_2CO_3, Sigma), cerium nitrate hexahydrate (99.99% $Ce(NO_3)_3 \cdot 6H_2O$, Aldrich), and molybdenum oxide (99.99% MoO_3, Aldrich). To make the precursor solution, K_2CO_3 and $Ce(NO_3)_3 \cdot 6H_2O$ were dissolved in water, and MoO_3 was dissolved in ammonium hydroxide solution. The precursor solution was dropped on the supported side of the Ni-$CoAl_2O_4$ or Ni-YSZ and calcined at 850 °C for 3 h. The microstructures of the cells were analyzed by field-emission scanning electron microscopy (FE SEM, Hitachi S4300SE, Hitachi, Tokyo, Japan). The potassium phase was identified by energy-dispersive X-ray spectrometry (EDX). XRD (Cu-Kα) and XPS (ESCALAB 220-IXL, Mg-Kα radiation) were used to analyze the phase state.

2. Cell Tests for Direct Internal Reforming of Methane

The hardware configuration for the button cell tests was presented in a previous paper [10]. After the anode in the button cell was reduced in a hydrogen flow at 850 °C for 8 h, methane humidified with a fixed steam content (steam to carbon ratio (S/C)=0.031 or 1.0) was introduced to the anode side at a constant flow rate. Normally, to prevent carbon coking, a large amount of steam (S/C≥2) is supplied with methane at the anode area and the cell is operated, but it is hard to measure cell deactivation in this condition and needs long time scale (over than 1,000 h). Therefore, humidified hydrogen or methane [steam to carbon ratio (S/C)=1.0] was supplied to the anode side with a total flow rate of 15 ml min^{-1}. This methane-rich composition is expected near the fuel inlet condition of the stack, where carbon-deposition is most likely to occur. To find out what differences exist between Ni-YSZ support and Ni-$CoAl_2O_4$ support, extremely low steam (3% H_2O) operations were also tested. Cell tests were carried out by flowing methane at 1.8 ml min^{-1} to the anode side and by loading 500 mA cm^{-2} current on the cell. This operating condition was obtained from theoretical calculation. If O^{2-} ions crossing over the electrolyte layer completely react with methane fuel, the exhaust is only CO and H_2 (Eq. (2)).

$$CH_4+O^{2-} \rightarrow 2e^-+CO+2H_2 \quad (2)$$

The cell voltage was monitored as a function of operating time under constant-current conditions. For the electrochemical characterization, a potentiostat with a frequency response analyzer (Solatron 1250/1268) was used and the AC-impedance was measured in the frequency range 1 MHz to 0.1 Hz with an amplitude of 10 mV. The gas composition of the exhaust was analyzed by gas chromatography (GC, Agilent 5890), using a thermal conductivity detector and a Carboxen-1000 column.

RESULTS AND DISCUSSION

1. DIR Tests with Cells with Ni-YSZ and Ni-$CoAl_2O_4$ Supports

Cell tests were carried out by feeding methane with a steam content of 3 vol% to the anode side at a flow rate of 1.8 mL min^{-1}. The cell voltage was monitored as a function of operating time while loading a constant current of 500 mA cm^{-2} at 850 °C. The changes in the cell voltage with time for 48 h of operation are shown in Fig. 1. Initially, the cell with the Ni-YSZ support exhibits a higher voltage than that with the Ni-$CoAl_2O_4$ support; it is already known that an Ni-YSZ support has a higher peak power density than that of Ni-$CoAl_2O_4$ [10]. After the reaction starts, Ni-YSZ shows a continuous drop of voltage with time and the voltage reaches almost 30% of the initial value in 48 h, after which the cell suffers a fracture. Ni-$CoAl_2O_4$ shows a rapid drop in the initial stage but later keeps a more or less constant voltage with time. The gas composition of the anode exhaust is shown in Table 1. The ratios of $H_2/(CO+CO_2)$ (4.64-7.13) with Ni-YSZ are much higher than those with Ni-$CoAl_2O_4$ (2.72-3.42). The ratios decrease steadily with time in both cases, resulting in less deposition of coke with time. If methane reforms

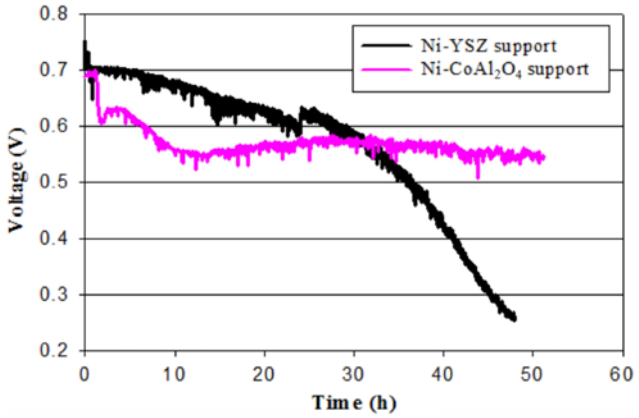

Fig. 1. Cell voltages versus time at constant current (500 $mAcm^{-2}$) for Ni-YSZ and Ni-$CoAl_2O_4$ supported cell operated in humidified (3% H_2O) methane at 850 °C.

Table 1. Gas composition (mole%) of the anode exhaust at different operating time

Anode support	Operating time (h)	CH_4	CO	CO_2	H_2	$H_2/(CO+CO_2)$	CO_2/CO	ΣC
Ni-YSZ	8	3.75	10.97	0.87	84.41	7.13	0.079	15.59
	27	4.31	14.29	1.13	80.28	5.21	0.079	19.73
	46	4.6	15.67	1.24	78.49	4.64	0.079	21.51
Ni-$CoAl_2O_4$	12	2.54	19.39	2.66	75.42	3.42	0.137	24.59
	29	3.7	21.94	3.4	70.56	2.78	0.155	29.04
	51	3.8	21.57	4.32	70.32	2.72	0.2	29.69

catalytically, the ratio of $H_2/(CO+CO_2)$ stays between 3 and 4, as the reforming proceeds by two steps:

$$CH_4+H_2O \leftrightarrow CO+3H_2 \quad (3)$$

$$CO+H_2O \leftrightarrow CO_2+H_2 \quad (4)$$

A mole ratio of $H_2/(CO+CO_2)$ higher than 4 with the Ni-YSZ support implies that there are reactions which deposit carbon on the support:

$$CH_4 \rightarrow C+2H_2 \quad (5)$$

$$2CO \rightarrow C+CO_2 \quad (6)$$

Table 1 shows that the total carbon (ΣC, the sum of CO, CO_2, and CH_4) detected in the exhaust of the Ni-YSZ support is much smaller than that detected in the exhaust of the Ni-$CoAl_2O_4$ support, indicating that Ni-YSZ has a higher degree of carbon deposition. This is why rapid deactivation is observed with Ni-YSZ supported cells. However, even for Ni-$CoAl_2O_4$, the methane concentration in the exhaust increases steadily with time as a result of a continuous decrease in the catalytic activity. This must be caused by a steady accumulation of coke, as evidenced by the increase in the total carbon value (ΣC) in the exhaust. The results obtained with Ni-$CoAl_2O_4$ are in agreement with reports that alumina-supported Co-Ni catalysts exhibit synergistic effects for methane/steam reforming and have superior carbon-deposition resistance compared to monometallic Ni/Al_2O_3 [19,20].

Interestingly, from Table 1, Ni-$CoAl_2O_4$ shows a ratio of $H_2/(CO+CO_2)$ less than 3 at later stages in the operation, when the steam reforming activity becomes low as a result of increased coke accumulation. One possible cause could be the existence of direct electrochemical oxidation of methane over the Ni-YSZ anode functional layer, as this gives an H_2/CO ratio=2.0 (Eq. (2)).

Another possibility is preferential electrochemical oxidation of H_2, rather than oxidation of CO, over the anode functional layer; this would result in a greater reduction in the H_2 content than in the CO content in the exhaust gas. With the present data, we do not know whether the two processes are occurring simultaneously or if only one of them is occurring. The CO_2/CO ratio with Ni-YSZ remains constant at 0.079, whereas the ratios with Ni-$CoAl_2O_4$ (0.137, 0.155, and 0.200) are higher than 0.079 and keep increasing with time. This is probably the result of an increased water-gas shift reaction **(4)** in the presence of Co; the activity of Co is less affected by coking. Another interesting point is why the functional anode layer of Ni-YSZ coated over the Ni-$CoAl_2O_4$ support does not experience deactivation, although the Ni-YSZ support shows rapid deactivation. This is probably because steam produced by electrochemical oxidation of H_2 at the functional anode layer of Ni-YSZ prohibits coke formation. Fig. 2 shows the profiles of gases through the anode layers. We expect the highest steam/carbon ratio at the electrolyte side of the anode functional layer and the lowest steam/carbon ratio at the fuel side of the anode support, where coke formation must be most severe.

2. Effects of K, Ce, and Mo Additives on Ni-$CoAl_2O_4$ Supports

The prevention of coke formation is very important in avoiding final fracture of the anode support caused by a steady accumulation of coke with operating time. To further improve the coke resistance, a small amount of a metal precursor such as K, Mo, or Ce was injected into the Ni-$CoAl_2O_4$ support. The melting point of K_2CO_3

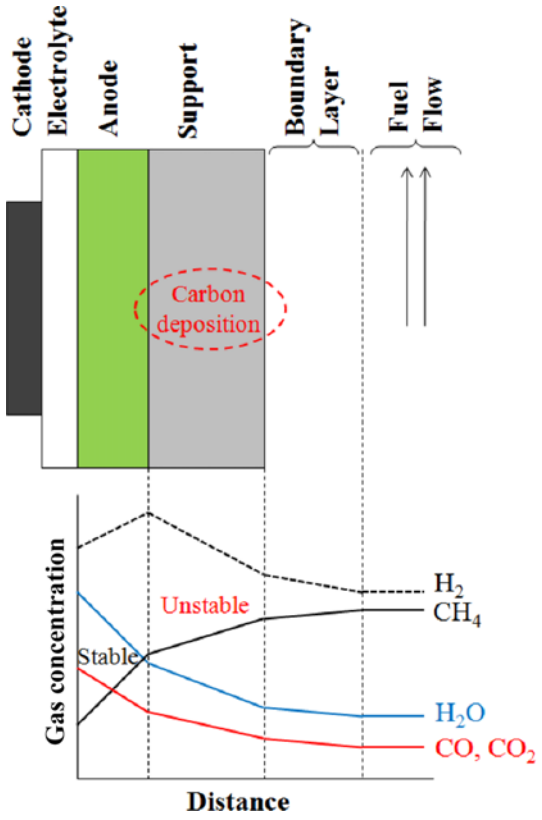

Fig. 2. Simplified profile of the gas composition versus distance during direct internal reforming operation. Functional anode layer is exaggerated for description of gas compositions.

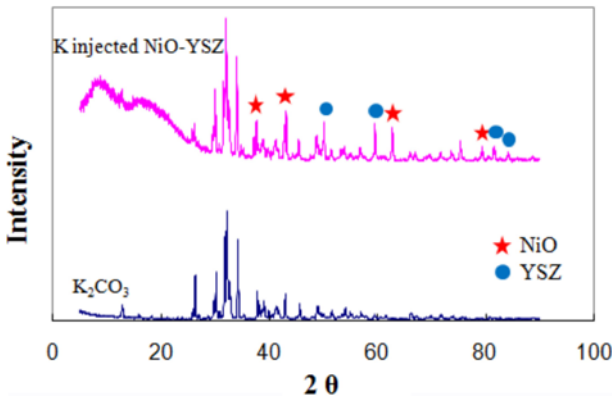

Fig. 3. X-ray diffraction patterns of K_2CO_3 (the bottom part) and 1 wt% K_2CO_3-injected Ni-YSZ cermet (the upper part).

is low, 891 °C; therefore, its chemical stability was checked after injection and calcination at 850 °C. Fig. 3 shows the XRD patterns of K_2CO_3 and the NiO-YSZ support injected with 1 wt% K_2CO_3. The results confirm that K_2CO_3 does not react with NiO or YSZ. Fig. 4 shows current-voltage curves of Ni-$CoAl_2O_4$ supported cells containing 0.5 wt% K_2CO_3, CeO_2, or MoO_3, measured with a feed of H_2 fuel (with 3 vol% H_2O). The open-circuit voltage (OCV) is stable for cells containing CeO_2 or MoO_3, but shows a small drop for K_2CO_3; the cell performance order is K_2CO_3>CeO_2>MoO_3. The cell with MoO_3 (not shown here) could not be tested under DIR conditions because the cell voltage was almost zero at a loading

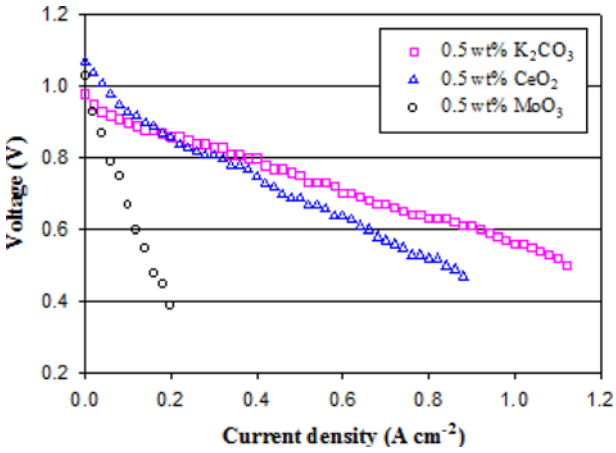

Fig. 4. Current-voltage curves of Ni-$CoAl_2O_4$ supported cells containing metal precursor of 0.5 wt% K_2CO_3, 0.5 wt% CeO_2 and 0.5 wt% MoO_3. Operated with hydrogen fuel (3 vol% steam) at 850 °C.

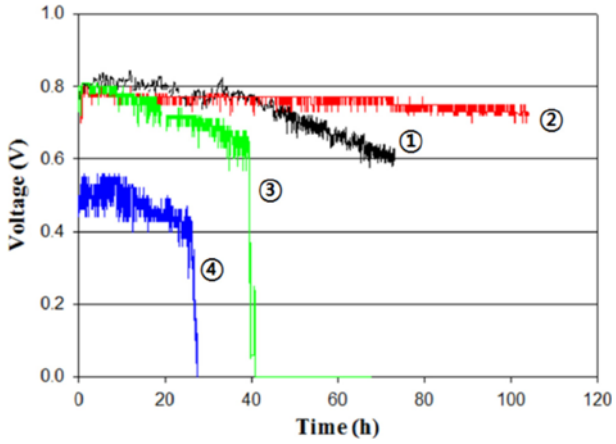

Fig. 5. Cell voltages versus time at constant current (400 $mAcm^{-2}$) for Ni-$CoAl_2O_4$ supported cells containing ① no additive, ② 0.5 wt% CeO_2, ③ 0.5 wt% K_2CO_3 and ④ 2 wt% K_2CO_3. Operated with steam/methane=1 at 850 °C.

current of 400 mA cm^{-2}.

Thus, only two samples of Ni-$CoAl_2O_4$, containing CeO_2 and K_2CO_3, were tested for the DIR reaction with a feed of humidified methane (steam/methane=1.0) at 850 °C. The results in Fig. 5 were obtained under a constant-current operating mode (400 mA cm^{-2}). For comparison, an Ni-$CoAl_2O_4$ support without additives was also tested. The cell containing CeO_2 shows the best stability up to 100 h. Addition of a small amount of CeO_2 seems to increase the activity of methane reforming and alleviate the carbon-deposition problem because CeO_2 has high oxygen mobility and a high oxygen-storage capacity [21-24]. The performance of K_2CO_3-injected cells is very poor: a steady drop in the voltage is accompanied by a sudden voltage drop to zero (not mechanical failure) in 40 h of operation for a cell with 0.5 wt% K_2CO_3, and in 27 h with 2 wt% K_2CO_3. The CO_2 selectivities for cells with K_2CO_3 are higher than those of other cells, and the values increase with increasing K_2CO_3 content, as shown in Table 2. The fast voltage drop for cells with K_2CO_3 seems to contradict the results of other studies, in which potassium was observed

Table 2. Effect of additive in Ni-$CoAl_2O_4$ supported cells on the gas composition (mole%) of the anode exhaust at different operating time

Anode support	Operation time (h)	CH_4	CO	CO_2	H_2
No additive	40	7.63	21.41	0.92	70.04
0.5% CeO_2	40	9.77	20.56	0.89	68.78
	100	8.75	20.21	0.86	70.18
0.5% K_2CO_3	30	9.41	18.6	1.44	70.55
2.0% K_2CO_3	25	4.47	17.49	2.28	75.77

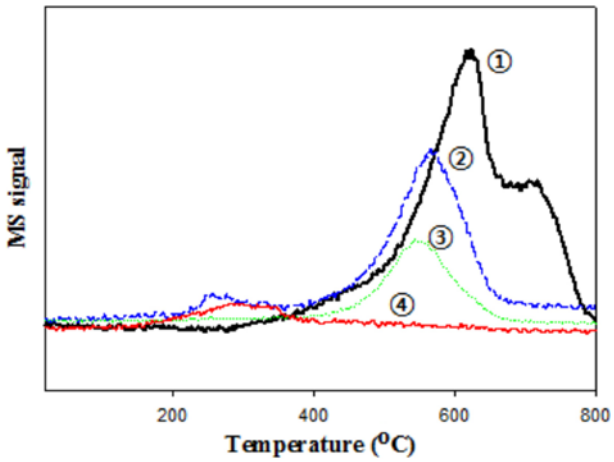

Fig. 6. TPO analyses of additive-incorporated Ni-$CoAl_2O_4$ supported cells that was operated at 850 °C under current density of 400 $mAcm^{-2}$ with a humidified methane (steam/methane =1) for 100 h. ① Ni-YSZ support; ② Ni-$CoAl_2O_4$ support; ③ Ni-$CoAl_2O_4$ with 0.5 wt% CeO_2; ④ Ni-$CoAl_2O_4$ with 0.5 wt% K_2CO_3.

to promote carbon removal during catalytic reforming over Ni [14-18]. We will see later that K does indeed remove coke effectively from the anode support and the voltage drop is not caused by carbon deposition.

The amount and type of the carbon deposit can be determined by temperature-programmed oxidation (TPO) of the used cell. After cell operation under a constant-current mode of 400 mA cm^{-2} for 100 h with methane fuel, the cell was cooled to room temperature in a flow of the same methane fuel, and then the amount of carbon deposit was measured by TPO in the temperature range of 20-800 °C. He with 10 wt% O_2 was fed to the anode side of the cell with a temperature-ramping rate of 10 °C min^{-1}. Fig. 6 shows the TPO results for various cells. For Ni-YSZ supported cells, the two peaks with the strongest intensities appear at 620 °C and 710 °C. For Ni-$CoAl_2O_4$ supported cells, one additional weak peak appears at 250 °C, together with a middle peak at 580 °C, but the highest-temperature peak at 710 °C is missing. The Ni-$CoAl_2O_4$ cell with a CeO_2 additive shows only one peak at 560 °C, and Ni-$CoAl_2O_4$ with a K_2CO_3 additive has only one weak peak at 300 °C. The CO_2 peak at 700 °C, detected only with the Ni-YSZ support, is responsible for the fast degradation of the cell performance. SEM analysis of the Ni-YSZ supported cell (Fig. 7(a)) reveals the existence of a large carbon lump encapsulating Ni, which is not seen in the Ni-$CoAl_2O_4$ supported

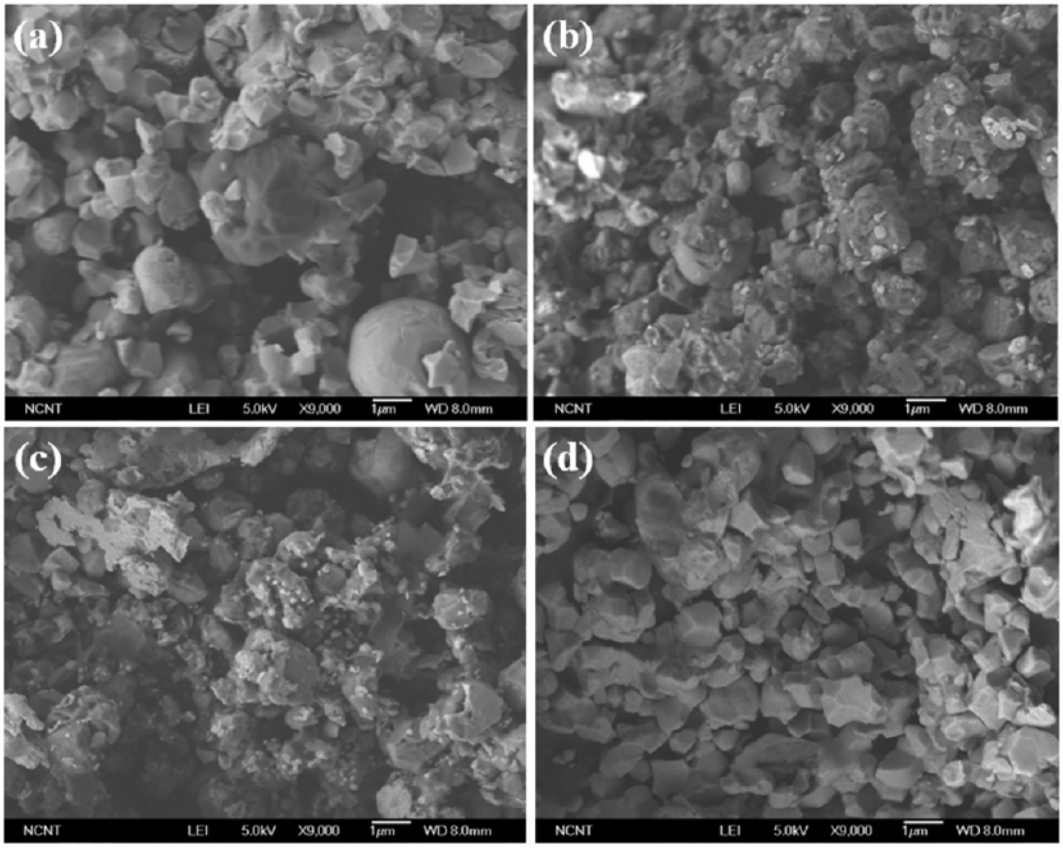

Fig. 7. SEM images of additive-incorporated Ni-$CoAl_2O_4$ supported cells that was operated at 850 °C under current density of 400 $mAcm^{-2}$ with a humidified methane (steam/methane=1) for 100 h. (a) Ni-YSZ support; (b) Ni-$CoAl_2O_4$ support; (c) Ni-$CoAl_2O_4$ with 0.5 wt% CeO_2; (d) Ni-$CoAl_2O_4$ with 0.5 wt% K_2CO_3.

cell (Fig. 7(b)). We therefore assign the peak at 700 °C to a bulky graphite-like carbon deposit. The SEM images of Ni-$CoAl_2O_4$ supported cells with and without CeO_2 (Fig. 7(b) and Fig. 7(c)) are similar in appearance, and have some surface roughness, probably as a result of the presence of active coke on the surface. The intensity of the middle peak at 560 °C is greatly reduced when CeO_2 is added to the Ni-$CoAl_2O_4$ support. The SEM image of Ni-$CoAl_2O_4$ with K_2CO_3 (Fig. 7(d)) shows only clean regular particles of NiO and $CoAl_2O_4$. We therefore assume that the peak at 300 °C does not originate from carbon deposition. This peak corresponds to strongly adsorbed CO_2 since this peak appears only for the Ni-$CoAl_2O_4$ supports without additives and the Ni-$CoAl_2O_4$ support with added K_2CO_3, all of which show enhanced CO_2 formation during DIR in the cell. It is now clear that the sudden voltage drop for cells with K_2CO_3 is not caused by carbon deposition.

3. Effects of Potassium on Cell Performance

Why is such unstable cell performance observed with K_2CO_3-injected cells, although there are no coke deposits on the anode support? K_2CO_3-injected cells exhibit several features: (1) no carbon is deposited; (2) the cells degrade suddenly to death; (3) the CO_2 selectivity of the exhaust gas increases proportionally with the amount of K_2CO_3; and (4) the peak power density increases by about 25%, but the OCV decreases in hydrogen fuel. To understand the effects of potassium, the current-voltage curves and impedance spectra were measured after 20 h of operation under a constant-current mode of 400 mA cm^{-2} with a feed of humidified H_2 fuel (3% steam). Fig. 8(a) shows the I-V curves of Ni-YSZ supported cells injected with various amounts of K_2CO_3. The cell performance increases from 0.5 to 0.67 Wcm^{-2} when 0.5-1 wt% K_2CO_3 is injected, whereas the OCV values decrease proportionally with increasing amounts of K_2CO_3. The impedance data in Fig. 8(b) show that when K_2CO_3 is injected the polarization resistance (R_{p_l}) decreases, whereas the electrolyte resistance (R_s) increases. Polarization resistance in the high-frequency range (R_{p_l}) is known for charge-transfer and surface reactions. We propose that K^+ ions in the anode promote the formation of OH^- ions, which accelerates the oxidation rate of hydrogen:

$$KOH \rightarrow K^+ + OH^- \quad (7)$$

$$2OH^- + H_2 \rightarrow 2H_2O \quad (8)$$

$$2K^+ + H_2O + O^{2-} \rightarrow 2KOH \quad (9)$$

It is already known that alkali promotes the adsorption of steam on nickel [25], and hydroxylated surfaces accelerate the anode reaction [26,27]. The decrease in the OCV with addition of K_2CO_3 can be explained by the existence of OH^- in the anode side, increasing the concentration of O^{2-} ions. The partial pressure of oxygen is known to be normally ultralow in the anode side ($P_{O_2} \leq 10^{-15}$ atm equiv.), and the OCV value is maximized under conditions of ultralow O_2 concentration in the anode side:

$$E = \frac{RT}{nF} \cdot \ln \frac{P_{O_2,cathode}}{P_{O_2,anode}} \quad (10)$$

Consequently, a small increase in the O_2 concentration in the anode effectively decreases the OCV value. The increase in the electrolyte resistance might be related to the diffusion of potassium to the electrolyte layer since potassium can spread through the grain boundary of the electrolyte [28-30]. In the presence of K^+ ions spread over cell layers, there must be a flow of OH^- ions because K^+ ions increase the concentration of OH^- ions at the anode side, and OH^- ions decrease at the cathode side because of the decomposition of OH^- ions to form water:

$$2OH^- + V_o \rightarrow H_2O + O_L^{2-} \quad (11)$$

Therefore, the direction of OH^- ion flow is opposite to the direction of O^{2-} ion flow, and this reduces the net ion current through the electrolyte. Fig. 9 depicts the mechanism on the change of cells after K addition.

To confirm the diffusion of anions in the presence of dispersed K^+ ions through the electrolyte layer, a mixture of CO_2 and O_2 (50 : 50) was fed to the cathode side of the K_2CO_3-containing Ni-YSZ supported cell while feeding H_2 fuel to the anode. We expected that CO_3^{2-} ions would be formed in the presence of K^+ ions at the cathode and diffuse from the cathode to the anode. Indeed, we succeeded in detecting CO gas in the fuel exhaust, and the amount increased with increasing K_2CO_3 content in the Ni-YSZ support, establishing that CO_3^{2-} ions move from the cathode to the anode, where CO is released to the anode exhaust:

$$CO_3^{2-} \rightarrow O^{2-} + CO(g) \quad (12)$$

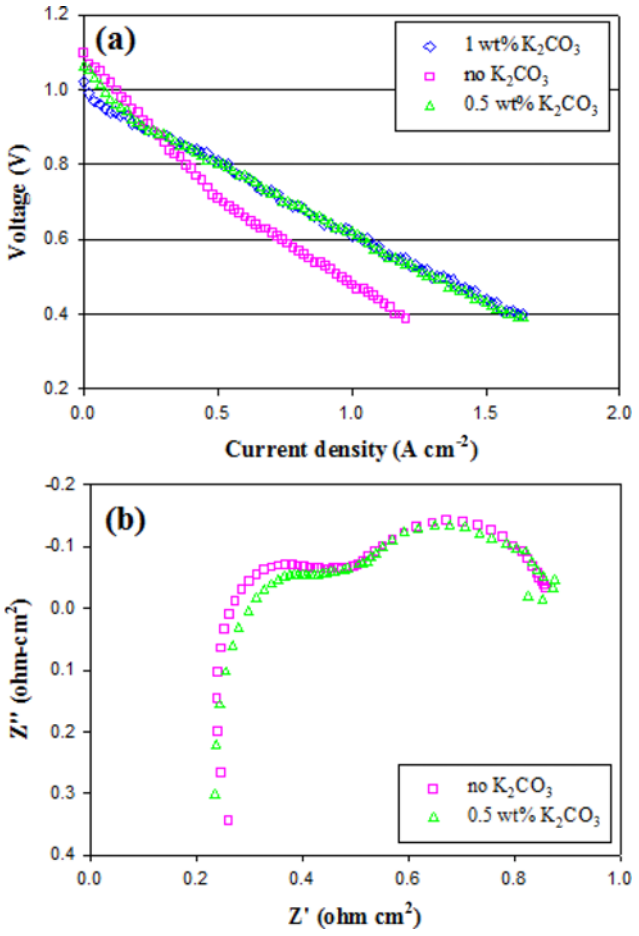

Fig. 8. (a) Current-voltage curves of Ni-YSZ supported cells containing different amount of K_2CO_3 (0 wt%, 0.5 wt% and 1 wt%). The cells were operated at 850 °C for 20 h with hydrogen fuel (3% steam) under current density of 400 mAcm^{-2}. (b) Impedance spectra of 0.5 wt% K_2CO_3-injected Ni-YSZ cell.

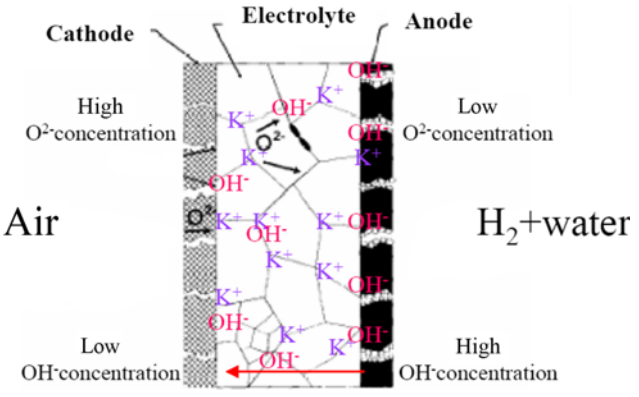

Fig. 9. Prospective model for potassium injected cell using hydrogen fuel.

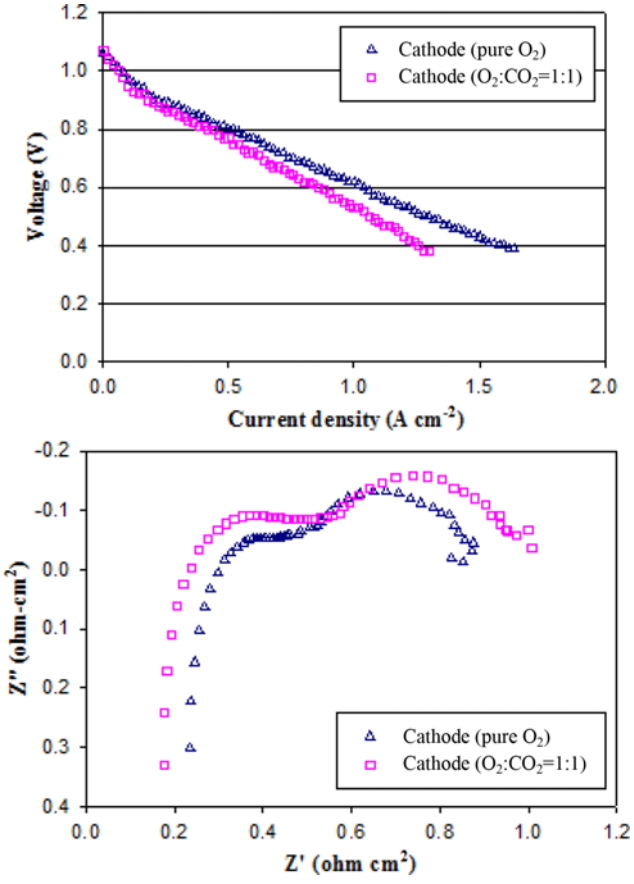

Fig. 10. Current-voltage curves and impedance spectra of 0.5 wt% K_2CO_3-injected Ni-YSZ supported cell. The cell was operated at 850 °C under current density of 400 mAcm^{-2} with H_2 fuel and pure O_2 for 20 h, then with H_2 fuel and a mixture of CO_2 and O_2 (50 : 40 mol%) for another 20 h.

Of course, no CO or CO_2 gas was detected without the presence of K_2CO_3 in the Ni-YSZ support, implying that CO_2 gas itself is not able to cross the electrolyte layer. Fig. 10 shows I-V curves and impedance spectra of K_2CO_3-injected Ni-YSZ cells while CO_2 is introduced to the cathode. After switching from pure O_2 to a mixture of CO_2 and O_2, the electrolyte resistance decreases, whereas the polarization resistances (Rp_1, Rp_2) increase and the cell performance is decreased by about 20%. From these results, it is established that CO_2 introduction to the cathode improves electrolyte resistance by increasing the flow of O^{2-} ions (CO_3^{2-}) from the cathode toward the anode, but interferes withO_2 adsorption and O^{2-} movement in the cathode. To confirm the effect of potassium on the cell, an Ni-YSZ supported cell containing no potassium was also tested, and the results are shown in Fig. 11. The impedance spectra show that the electrolyte resistance does not change when CO_2 is injected, but the polarization resistance increases. This confirms again that potassium ions that have infiltrated the electrolyte and cathode layers help CO_3^{2-} or OH^- ions to cross over the electrolyte layer. XPS measurements to detect potassium in the anode functional layer were conducted with Ni-YSZ supported cells with injection of 5 wt% K_2CO_3. With 1-2 wt% K_2CO_3 injection, XPS could not detect the potassium peaks, probably because of a sensitivity problem. Fig. 12 confirms the presence of potassium, yttrium, and carbon elements

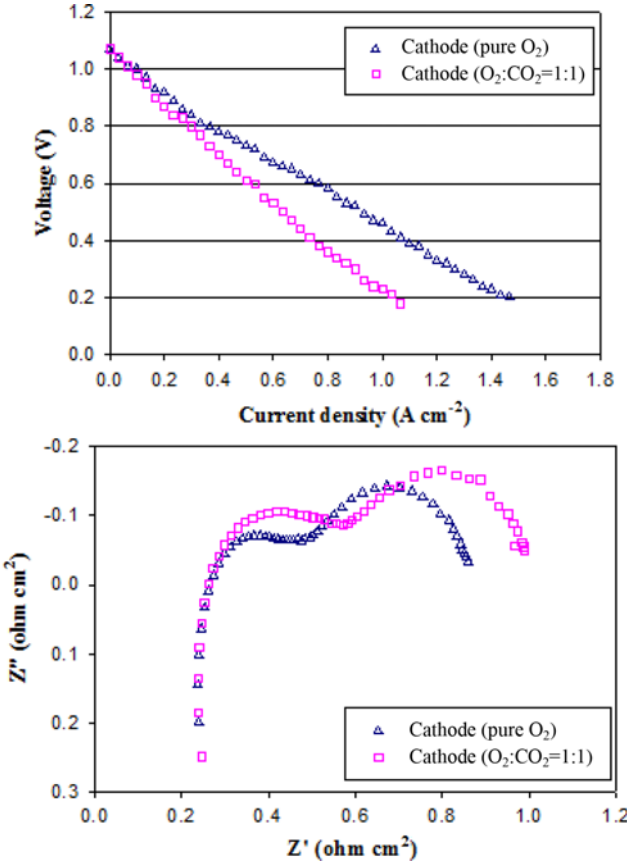

Fig. 11. Current-voltage curves and impedance spectra of Ni-YSZ supported cell. The cell was operated at 850 °C under current density of 400 mAcm^{-2} with H_2 fuel and pure O_2 for 20 h, then with H_2 fuel and a mixture of CO_2 and O_2 (50 : 40 mol%) for another 20 h.

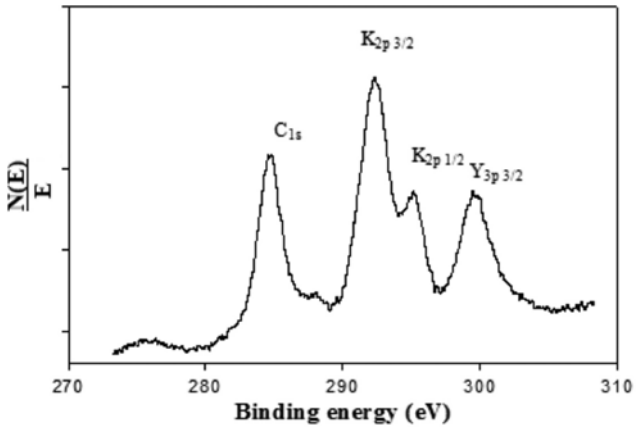

Fig. 12. XPS result of 5 wt% K_2CO_3-injected Ni-YSZ supported cell that have been operated at 850 °C under current density of 400 mAcm^{-2} with H_2 fuel for 20 h. X-ray beam targets on the YSZ electrolyte layer.

in the anode functional layer. The carbon must come from carbonate ions (CO_3^{2-}) remaining in the YSZ layer.

It is now clear that, for K_2CO_3-containing Ni-$CoAl_2O_4$ supported cells, K^+ ions in the anode side promote the generation of OH^- under H_2 fuel conditions, and of CO_3^{2-} under methane-reforming conditions. K^+ ions that have infiltrated through the electrolyte layer to the cathode now facilitate the dissolution of these ions and must promote diffusion up to the cathode side. Thus, in DIR operation, counter-current flow of O^{2-} (in OH^- or CO_3^{2-}) from the anode toward the cathode will increase the resistance of the YSZ electrolyte layer. CO_3^{2-} ions diffused to the cathode decompose to produce CO_2 and O^{2-} ions over oxygen vacancies in the cathode. In DIR operation, therefore, two unfavorable factors deteriorate the cell performance with time. First, the polarization resistance of the cathode keeps increasing as a result of increased occupation of K^+ ions and increased CO_3^{2-} ion species. Secondly, the electrolyte resistance also keeps increasing with time since a more even distribution of K^+ ions throughout the cathode and electrolyte layers will increase the counter-diffusion of O^{2-} ions from the anode to the cathode. Saturation of polarization resistance, which minimizes the activity of the cathode, coupled with the maximized electrolyte resistance results in a balance between the diffusion of O^{2-} and the counter-diffusion of OH^- and CO_3^{2-}; the cell may experience a sudden drop in voltage after a certain period of time. This period decreases as the amount of K_2CO_3 increases.

CONCLUSIONS

Button cells of Ni-YSZ/YSZ/LSM were supported on two different layers of Ni-YSZ or on Ni-$CoAl_2O_4$. These cells were used for internal reforming of methane with a feed of humidified methane (3 vol% steam) and air to the anode and cathode, respectively, at 850 °C under a constant current of 500 mA cm^{-2}. Ni-YSZ supported cells deactivate quickly and suffer fracture in 50 h. Ni-$CoAl_2O_4$ supported cells show little degradation with operating time because of their higher resistance against carbon deposition. Upon incorporation of additives such as K, Ce, and Mo into the Ni-$CoAl_2O_4$ support, the cell containing 0.5 wt% CeO_2 exhibits the best stable per-

formance during 100 h of operation. The cell with 0.5 wt% Mo exhibits the worst performance, showing almost zero voltage under a current loading of 400 mA cm^{-2}. The cells with K_2CO_3 additives show mixed performance compared with those of cells without additives: a better performance is obtained with an H_2 fuel feed, especially in the high-current region, but the performance with methane fuel is worse. When operated under constant-current mode, they show steady decreases in the voltage, accompanied by a sudden voltage drop to zero in 40 h of operation for the cell with 0.5 wt% K_2CO_3 and in 27 h with 2 wt% K_2CO_3. TPO and SEM measurements of used cells reveal that Ni-YSZ supported cells experience severe coke deposition of surface carbon, with a TPO peak at 560 °C, and formation of a bulky carbon lump that encapsulates Ni particles, with a TPO peak at 700 °C. Ni-$CoAl_2O_4$ supports with and without CeO_2 have much smaller amounts of coke deposition, with a TPO peak at around 560 °C; the latter shows 50% more reduction in coke accumulation, thus showing better stability during cell operation. Ni-$CoAl_2O_4$ with K_2CO_3 does not result in any coke accumulation on the surface, as evidenced by the SEM image, and shows only one weak TPO peak at 300 °C. The low-temperature peak at around 250-300 °C that appears in two samples, i.e., Ni-$CoAl_2O_4$ and Ni-$CoAl_2O_4$ with K_2CO_3, correlates with increased CO_2 concentration in the anode exhaust and is assigned to strongly adsorbed CO_2.

The continuous voltage drop and final failure of cell operation in the case of K_2CO_3-injected Ni-$CoAl_2O_4$ supports is caused by the spread of K^+ ions to the electrolyte and cathode layers and accompanying diffusion of OH^- and CO_3^{2-} ions from the anode toward the cathode. There is a steady increase with time of polarization resistance at the cathode as a result of accumulation of K^+ ions, CO_3^{2-} ions, and increased loss of oxygen vacancies. Finally, the cathode reaches a saturation point with a minimized active site, resulting in operation failure, coupled with increased electrolyte resistance caused by counter-diffusion of OH^- and CO_3^{2-} ions.

ACKNOWLEDGEMENTS

The authors would like to thank the Ministry of Trade, Industry and Energy (20093020030030) and BK21 program of Korea for financial support.

REFERENCES

1. A. L. Lee, R. F. Zabransky and W. J. Huber, *Ind. Eng. Chem. Res.*, **29**, 766 (1990).
2. I. Gavrielatos, V. Drakopoulos and S. G. Neophytides, *J. Catal.*, **259**, 75 (2008).
3. R. M. Ormerod, *Stud. Surf. Sci. Catal.*, **122**, 35 (1999).
4. N. C. Triantafyllopoulos and S. G. Neophytides, *J. Catal.*, **217**, 324 (2003).
5. T. Borowiecki, A. Golebiowski and B. Stasinska, *Appl. Catal. A: Gen.*, **153**, 141 (1997).
6. C. M. Finnerty, N. J. Coe, R. H. Cunningham and R. M. Ormerod, *Catal. Today*, **46**, 137 (1998).
7. V. D. Belyaev, T. I. Politova, O. A. Marina and V. A. Sobyanin, *Appl. Catal. A: Gen.*, **133**, 47 (1995).
8. Y. Lin, Z. Zhan and S. A. Barnett, *J. Power Sources*, **158**, 1313 (2006).
9. N. Laosiripojana and S. Assabumrungrat, *Appl. Catal. B: Environ.*, **66**, 29 (2006).
10. B. H. Kwak, H. K. Youn and J. S. Chung, *J. Power Sources*, **185**, 633 (2008).
11. N. Laosiripojana and S. Assabumrungrat, *Appl. Catal. B: Environ.*, **60**, 107 (2005).
12. N. Laosiripojana, W. Sangtongkitcharoen and S. Assabumrungrat, *Fuel*, **85**, 323 (2006).
13. N. Laosiripojana and S. Assabumrungrat, *Appl. Catal. A: Gen.*, **290**, 200 (2005).
14. J. R. Rostrup-Nielsen and L. J. Christiansen, *Appl. Catal. A: Gen.*, **126**, 381 (1995).
15. J. Juan-Juan, M. C. Roman-Martinez and M. J. Illan-Gomez, *Appl. Catal. A: Gen.*, **264**, 169 (2004).
16. J. Juan-Juan, M. C. Roman-Martinez and M. J. Illan-Gomez, *Appl. Catal. A: Gen.*, **301**, 9 (2006).
17. P. O. Graf, B. L. Mojet and L. Lefferts, *Appl. Catal. A: Gen.*, **346**, 90 (2008).
18. K. M. Hardiman, C. G. Cooper and A. A. Adesina, *Ind. Eng. Chem. Res.*, **43**, 6006 (2004).
19. K. Opoku-Gyamfi, Zahra M. Tafrechi and A. A. Adesina, *React. Kinet. Catal. Lett.*, **64**, 229 (1998).
20. B. C. Enger, R. Lødeng and A. Holmen, *Appl. Catal. A: Gen.*, **346**, 1 (2008).
21. A. Al-Ubaid and E. E. Wolf, *Appl. Catal.*, **40**, 73 (1998).
22. M. Mogensen, N. M. Sammes and G. A. Tompsett, *Solid State Ionics*, **129**, 63 (2000).
23. P. Fornasiero, G. Balducci, R. D. Monte, J. Kaspar, V. Sergo, G. Gugitosa, A. Ferrero and M. Graziani, *J. Catal.*, **164**, 173 (1996).
24. T. Miki, T. Ogawa, M. Haneda, N. Kakuta, A. Ueno, S. Tateishi, S. Matsuura and M. Sato, *J. Phys. Chem.*, **94**, 6464 (1990).
25. N. D. Lang, S. Holloway and J. K. Norskov, *Science*, **236**, 403 (1987).
26. S. Raz, K. Sasaki, J. Maier and I. Riess, *Solid State Ionics*, **143**, 181 (2001).
27. J. Mizusaki, H. Tagawa, T. Saito, T. Yamamura, K. Kamitani, K. Hirano, S. Ehara, T. Takagi, T. Hikita, M. Ippommatsu, S. Nakagawa and K. Hashimoto, *Solid State Ionics*, **70/71**, 52 (1994).
28. A. L. Dicks, *J. Power Sources*, **61**, 113 (1996).
29. H. Praliaud, J. A. Dalmon, C. Mirodatos and G. A. Martin, *J. Catal.*, **97**, 344 (1986).
30. J. R. Rostrup-Nielsen and L. J. Christiansen, *Appl. Catal. A: Gen.*, **126**, 381 (1995).